analytical chemistry

pubs.acs.org/ac Article

Direct Detection of Uranyl in Urine by Dissociation from Aptamer-Modified Nanosensor Arrays

Reut Meir, Marina Zverzhinetsky, Nimrod Harpak, Ella Borberg, Larisa Burstein, Offer Zeiri, Vadim Krivitsky,* and Fernando Patolsky*

Cite This: *Anal. Chem.* 2020, 92, 12528–12537 Read Online

ACCESS | Metrics & More | Article Recommendations | Supporting Information

ABSTRACT: An ever-growing demand for uranium in various industries raises concern for human health of both occupationally exposed personnel and the general population. Toxicological effects related to uranium (natural, enriched, or depleted uranium) intake involve renal, pulmonary, neurological, skeletal, and hepatic damage. Absorbed uranium is filtered by the kidneys and excreted in the urine, thus making uranium detection in urine a primary indication for exposure and body burden assessment. Therefore, the detection of uranium contamination in bio-samples (urine, blood, saliva, etc.,) is of crucial importance in the field of occupational exposure and human health-related applications, as well as in nuclear forensics. However, the direct determination of uranium in bio-samples is challenging because of "ultra-low" concentrations of uranium, inherent matrix complexity, and sample diversity, which pose a great analytical challenge to existing detection methods. Here, we report on the direct, real-time, sensitive, and selective detection of uranyl ions in unprocessed and undiluted urine samples using a uranyl-binding aptamer-modified silicon nanowire-based field-effect transistor (SiNW-FET) biosensor, with a detection limit in the picomolar concentration range. The aptamer-modified SiNW-FET presented in this work enables the simple and sensitive detection of uranyl in urine samples. The experimental approach has a straight-forward implementation to other metals and toxic elements, given the availability of target-specific aptamers. Combining the high surface-to-volume ratio of SiNWs, the high affinity and selectivity of the uranyl-binding aptamer, and the distinctive sensing methodology gives rise to a practical platform, offering simple and straightforward sensing of uranyl levels in urine, suitable for field deployment and point-of-care applications.

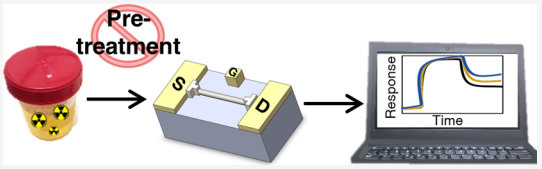

The growing demand for uranium-based nuclear power,[1] and the resulting wide-spread processing and transportation of uranium, raises concerns about the environmental impacts and risks for human health. The general population is mainly exposed to uranium via the ingestion of drinking water and food that contain uranium. People living in close vicinity to uranium mines are at higher risk for exposure from these sources because of the elevated uranium concentrations in soils.[2] Occupational exposures, both chronic and acute, may take place throughout the uranium production industry, from mining and milling to nuclear fuel fabrication,[2] as well as in nuclear weapon development and additional medical and industrial fields. Exposure to depleted uranium, a by-product of uranium enrichment processes used in military armors and munition, may occur through embedded shrapnel or inhalation of aerosols produced during munition impacts.[2] Toxicological effects related to uranium intake (natural, enriched or depleted uranium) depend on its chemical form and exposure route, and primarily involve renal damage, however, pulmonary, neurological,[3] skeletal, and hepatic effects are also possible as absorbed uranium accumulates in the related organs. Additionally, inhaling insoluble uranium compounds increases the risk for internal chronic exposure of the lungs mainly to alpha radiation. Roughly 67% of absorbed uranium (i.e., in the blood) is filtered by the kidneys and excreted in urine within 24 h, and as much as 90% is excreted in total. Thus, uranium detection in urine is crucial for exposure and body burden assessment. Urinary uranium excretion can provide a rapid and sensitive indication for exposure to ingested, inhaled, or embedded uranium. Moreover, uranium detection in biological samples, such as urine and blood, can be used in nuclear forensics to obtain valuable information about individuals who were involved in handling nuclear materials, provide authorities with the information required for prosecution, and assist in minimizing the illegal proliferation of radioactive materials.[4]

Nevertheless, the direct determination of uranium in bio-samples is challenging, owing to the following reasons: (i) bio-samples often contain extremely low concentrations of uranium. In the National Health and Nutrition Examination Survey (NHANES), 2001−2010, conducted in the United States, urinary uranium concentrations of 9025 unexposed US citizens of various ages and ethnicities averaged 17.3 ng/L (71

Received: June 4, 2020
Accepted: August 26, 2020
Published: August 26, 2020

https://dx.doi.org/10.1021/acs.analchem.0c02387
Anal. Chem. 2020, 92, 12528−12537

pM) with a median of 9 ng/L (36 pM). Urinary uranium concentrations of another 3147 citizens (26% of the sample) were below the detection limit of the analytical method (inductively coupled plasma mass spectrometry, ICP−MS) which was 1.7 ng/L (6.9 pM).[5] (ii) Bio-samples are complicated matrices, containing high concentrations of organic and inorganic materials, which may hinder selectivity and sensitivity. (iii) By their nature, bio-samples may greatly differ from one specimen to another, because of different pH, nutrient content, dilution, and so forth, rendering them difficult to obtain a generic procedure to fit all cases. Thus, these low uranium concentrations, along with the inherent complexity of bodily fluids, pose a great analytical challenge to existing detection methods.

In the context of uranium detection in urine, ICP−MS is a common analytical method of choice in many laboratories worldwide.[6] It is a well-established, highly sensitive, robust, and reliable analytical method. Nevertheless, ICP−MS for urine analysis must be performed in a laboratory, by trained personnel, and sample preparation is often needed (might be laborious and time consuming or simple as sample dilution[6]). The significance of ICP−MS is far from being undermined by other methods, yet the need for complementary simple, fast, and reliable point-of-care quantification methods for uranium in urine is still an unmet challenge.

A recently published review by Wu et al.[7] thoroughly surveys the myriad of uranyl (UO_2^{2+}) sensing methods that have been reported over the years, including optical, electrochemical, and other types of methods.[7] Uranyl is the most stable chemical form of uranium in water and the most abundant in biological fluids. The core of these methods is the combination of a recognition component and a reporter component, that is, a uranyl-specific receptor (e.g., macrocyclic host molecules including crown ethers, calixarenes,[8−10] carboranes,[11] etc.,), and a mechanism by which information regarding uranyl detection is transformed into a readable and measurable output quantity (e.g., light absorption, voltage, current, etc.). Despite many methods achieving impressive limits of detection as low as 0.1 nM (and several with 10, 1, and 0.1 pM) for uranyl in water samples of various sources and complexities, none of the reported sensors was used to measure uranyl in either urine or blood.

One of the most prominent methods[12] utilized a uranyl-selective DNAzyme, as the receptor. DNAzymes are DNA molecules with enzymatic activities. The reported DNAzyme, first introduced by Liu et al.[13] in 2007, displayed excellent specificity against other metals. It was found that upon uranyl binding, it can cleave an RNA-site embedded in a matching DNA strand, thus leading to the release of a DNA strand, which can further undergo detection, reporting the presence of uranyl. Following Liu's work, this DNAzyme was further characterized and derivatized,[14,15] giving rise to a number of cleavage-based methods, utilizing various reporting mechanisms, such as colorimetry,[16] fluorimetry, spectrophotometry, electrochemistry, resonance light scattering,[17] and so forth, showing very good detection limits. In one scarce noncleavable derivative,[18] the cleavable ribonucleic site was replaced with a similar deoxyribonucleic site, eliminating the cleavability of the molecule, and practically yielding a uranyl-binding aptamer (HS-DNA 1), displaying a strong affinity toward uranyl, and good extraction capabilities. Aptamers are known to be a special class of easily prepared nucleic acids that can specifically bind, with a high affinity, to a given target molecule.

Over the past two decades, silicon nanowire-based field-effect transistors (SiNW-FETs) have been demonstrated as powerful sensors for the detection of both chemical and biological species.[19−43] The intrinsically high surface-to-volume ratio 1D-NW building blocks are incorporated into FETs, yielding devices that are extremely sensitive to the adsorption of charged species on their surface. These charged species induce a field-gating effect on the charge carriers within the NWs, causing significant changes in their resulting electrical conductance.

Until recently, the applicability of FETs for direct measurement in biological fluids was highly hindered by the extremely high ionic strength and the plethora of organic and inorganic species that mask the field effect induced by the target molecules. In 2016, Krivitsky et al.[24] demonstrated that given a specific high-affinity receptor immobilized to the surface of the SiNWs, high sensitivity in biosamples can be achieved using a "dissociation-mode regime", which exploits the temporal differentiation between the desorption of the target molecule and the nonspecifically bound molecules, which comprise the biosample. Accordingly, the utilization of immobilized aptamers, as selective and strong-binding receptors, combined with the dissociation-mode regime, can be expected to enable direct sensing of chemical species in undiluted biosamples. While aptamer-modified SiNW-FETs have been utilized for the detection of dopamine,[44,45] neuropeptide Y,[44] thrombin,[46,47] vascular endothelial growth factor,[48] and potassium ion,[49] none of which demonstrated measurement in undiluted biological fluids.

Here, we report the direct, real-time, sensitive, and selective detection of uranyl ions in unprocessed and undiluted urine samples using a uranyl-binding aptamer-modified SiNW-FET biosensor, with a detection limit in the picomolar (pM) concentration range.

EXPERIMENTAL SECTION

Materials and Chemicals. 1-Ethyl-3-(3-dimethylaminopropyl)carbodiimide (EDC), *N*-hydroxysulfosuccinimide sodium salt (sulfo-NHS), anhydrous toluene, glycine, hydrochloric acid (HCl), phosphate-buffered saline (PBS) tablets, potassium phosphate monobasic, and potassium phosphate dibasic were purchased from Sigma-Aldrich and were used as received. 3-Hydroxypropionic acid was purchased from Shanghai Aoyeah chemicals Technology. (3-Aminopropyl)-dimethyl-ethoxysilane (APDMES) was purchased from Gelest Inc. Carboxy-terminated ssDNA aptamer (5′-COOH-CTGCA GAATT CTAAT ACGAC TCACT ATAGG AAGAG ATGGC GACAT CTCTG CAGTC GGGTA GTTAA ACCGA CCTTC AGACA TAGGC AGGCG TATAT CTTGT GACGG TAAGC TTGGC AC-3′) was purchased from Integrated DNA technologies. Deionized water (18 MΩ·cm) was used for all procedures. Uranyl acetate dihydrate was dissolved in water to obtain a 1×10^{-3} M uranyl stock solution.

Spot urine samples were collected from healthy volunteers and were used within 10 h from collection. A 12-parameter urine test strip (DUS 12AC, One Step) was used to qualitatively verify that urine samples were within the normal levels. Prior to use, urine was filtered using a 0.45 μm syringe-filter with a cellulose acetate membrane.

p-Type SiNW Synthesis. The synthesis of SiNWs by chemical vapor deposition was performed as previously described.[50] Briefly, 20 nm gold nanoparticles (Ted Pella)

https://dx.doi.org/10.1021/acs.analchem.0c02387
Anal. Chem. 2020, 92, 12528−12537

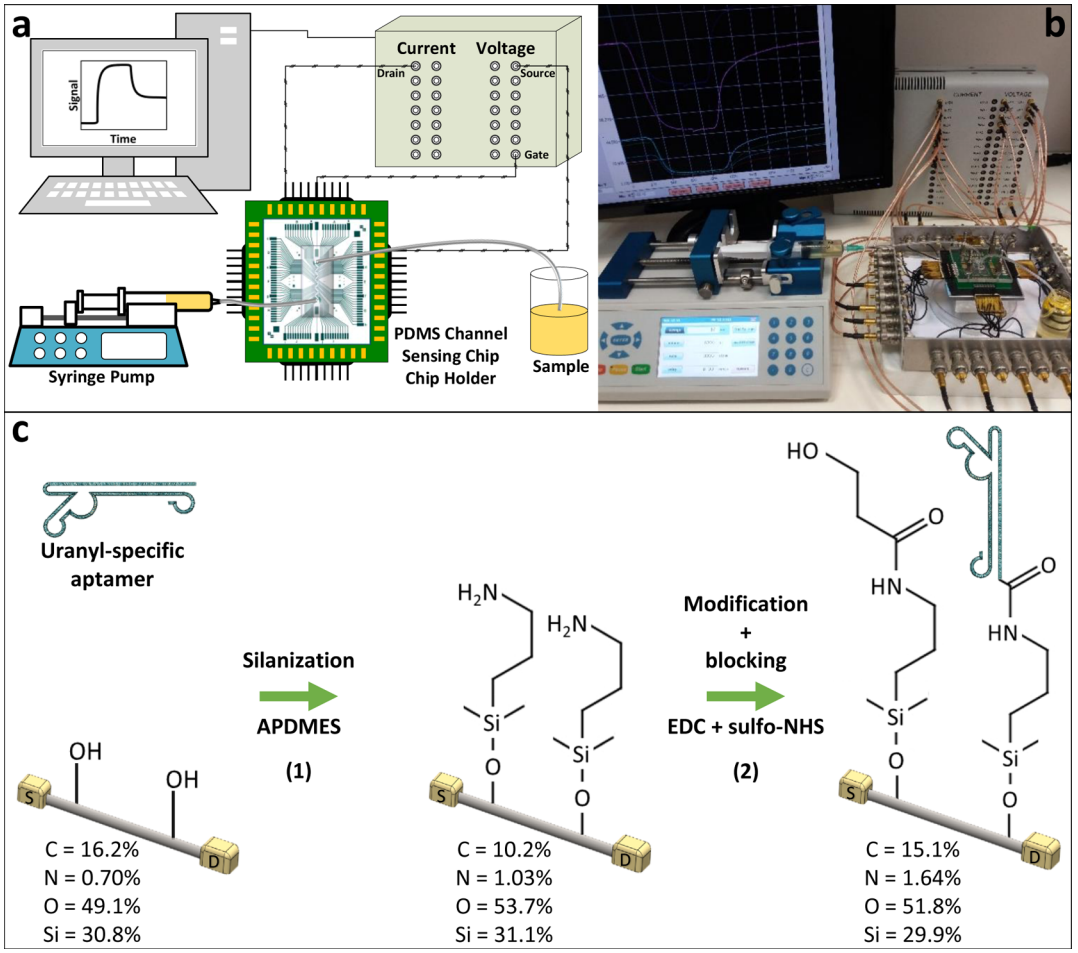

Figure 1. (a) Schematic representation and (b) image of the experimental setup. (c) Surface modification, XPS analysis, and chip configuration of the uranyl-binding aptamer-modified SiNW-FET. The stages of the surface modification: (1) silanization of the SiNW-activated surface with amine groups; (2) amine-terminated surface reaction with the carboxy-terminated aptamer after EDC and sulfo-NHS activation, followed by blocking with similarly activated 3-hydroxypropionic acid. The atomic concentrations, measured by XPS analysis, of the modified surface [for carbon (C), nitrogen (N), oxygen (O), and silicon (Si)], are denoted for each step of the modification.

were used to catalyze the growth of SiNWs via the vapor−liquid−solid mechanism. These nanoparticles were first deposited on silicon (1 0 0) growth substrates to define sites for SiNW growth. In order to assist the attachment of the gold nanoparticles to the silicon substrate, a layer of poly-L-lysine (Ted Pella) was first introduced to the silicon wafer and served as an electrostatic binding agent. The organic materials were removed by applying oxygen plasma (100 W, 0.2 Torr) for 5 min. Next, the wafer was placed in a quartz tube furnace, where silane (SiH_4) and diborane (B_2H_6, 100 ppm in H_2 balance gas) were used as reactants for the SiNW growth process, in which boron served as a p-type dopant with a boron/silicon ratio of 1/4000. The rate of the SiNW growth was ∼1 μm/min.

SiNW-FET Array Fabrication. The SiNW-FET array was fabricated in a cleanroom by photolithography and metal deposition as previously described,[50] with the following changes: after fabrication of the outer electrodes (including the gate) by photolithography and evaporation of chromium/gold (5 nm/60 nm), on a 3 in. silicon wafer, covered with a 600 nm thermal oxide layer (<0.005 Ω/cm, SSP prime grade, Silicon Quest International), the p-type SiNWs were deposited on the wafer by dispersion in ethanol and dispensing 0.5 μL drops on top of the oxide layer. Source and drain electrodes of FETs were defined with a multilayer photoresist structure consisting of 500 nm LOR5A (Microchem) and 500 nm S1505 (Microchem). Notably, the gap between the source and drain electrodes was 3 μm. Following exposure and development in an AZ726 developer (Merck), the chip was dipped in a buffered oxide etchant (1:6 hydrofluoric acid/ammonium fluoride, Transene) for 7 s, washed in deionized water, and immediately metalized by e-beam evaporation of titanium/palladium/titanium (10 nm/80 nm/5 nm). Subsequently, electrodes were insulated with a layer of 10 nm alumina, made by atomic layer deposition (Savannah 200 system, Cambridge Nanotech). The chip was then subjected to lift-off in *N*-methyl-2-pyrrolidone (JT Baker).

Electrical Characterization. Prior to surface modification, fabricated devices were characterized using a probe station (Janis Research Co., Washington), with deionized water as a water gate.[50] This characterization procedure was mainly intended to evaluate the device quality and yield, and choose the best devices for upcoming sensing experiments. The *I*−*V* characteristics of each device were evaluated by measuring the source−drain current (I_{sd}) response to the applied source−drain voltage (V_{sd}), which was varied between −0.2 and 0.2 V at a constant gate voltage (V_g). The measurement was repeated for gate voltages varying from −0.5 to 0.2 V (Figure S1a). Using the results of the V_{sd}-sweep measurements, a V_{sd}

https://dx.doi.org/10.1021/acs.analchem.0c02387
Anal. Chem. 2020, 92, 12528−12537

allowing full-scale sensitivity was selected. The gate-dependent I_{sd} of the devices was measured at a V_{sd} of 0.3 V for V_g varying from −0.3 to 0.3 V (Figure S1b). The slope of the curve's linear region is the transconductance of the devices and serves as a measure of its sensitivity. Devices that displayed low transconductance were dimmed insensitive and were not used for further experiments. On average, out of 100 potential devices per chip, about 20% are usually found adequate for sensing experiments. The best performing devices were selected and mapped for later use in the uranyl-sensing experiments.

Polydimethylsiloxane Microfluidic Channel Fabrication. The fabrication of the fluid-delivery device from the flexible polydimethylsiloxane (PDMS, Sylgard) elastomer was performed as previously described,[50] with the following changes: PDMS was incubated overnight with a curing agent at a 10:1 mass ratio at 60 °C. The resulting device was then cut into rectangular 10 × 10 × 5 mm ($W \times L \times H$) pieces. The embedded channel was rectangular, with inlet and outlet holes and dimensions of 1 × 5 × 0.1 mm ($W \times L \times H$).

Aptamer Modification. Following the SiNW-FET array fabrication and characterization, the carboxy-terminated DNA aptamer was immobilized to the SiNW surface. First, the chip was successively washed with acetone, isopropanol, and deionized water, followed by nitrogen drying. Then, oxygen plasma cleaning was applied for 7 min at 100 W. The chip was transferred into a glovebox under an argon atmosphere (water and oxygen-free) to apply the amino-silane modification. Immediately afterward, the chip was covered with ∼200 μL APDMES for 60 min. The chip was then washed three times with ∼4 mL of anhydrous toluene. Immersed in clean toluene, the chip was transferred from the glovebox to a cleanroom and washed with isopropanol followed by nitrogen drying. Next, the chip was placed on a hot plate at 115 °C for 30 min. At this point, the chip was mounted on a chip carrier and selected devices were wire bonded to the chip carrier's contact pads. A PDMS microfluidic channel was assembled on top of the chip, confining the area of the devices and enabling directed liquid flow over the analytical zone, using a syringe pump and tubing.

To activate its carboxylic acid residue, the aptamer was reacted with EDC and sulfo-NHS in PBS (pH 7), for 20 min. Then, the activated-aptamer solution was drawn through the microfluidic channel over the amine-terminated SiNWs. After 2 h, phosphate buffer (PB) was drawn through the channel, in order to remove any unreacted aptamers and reaction byproducts. Similarly, 3-hydroxypropionic acid was also reacted with EDC and sulfo-NHS in PB (adjusted to pH 6.5 using NaOH) and drawn through the microfluidic channel in order to block unreacted amine residues. Finally, the channel was washed with PB followed by a thorough wash with deionized water to remove reaction byproducts. The chip was air dried and stored at 4 °C, when not in use.

Sample Preparation. Phosphate buffers (pH 7) were prepared by mixing equimolar ratios of potassium phosphate monobasic and potassium phosphate dibasic at 10 mM (PB), and 0.1 mM (sensing buffer, SB). Either SB or urine was spiked with increasing concentrations of uranyl acetate in order to prepare the calibration samples. Spiked urine samples were measured as prepared, without any pretreatment or dilution.

Experimental Setup and Data Acquisition. The sensing chip was mounted on a chip carrier and the best-performing devices were wire-bonded (using a wire-bonder, model 8850, West Bond). The custom-made PDMS microfluidic channel was installed on top of the sensing chip and connected to a syringe pump (Fusion 200, Chemyx) using a Tygon tubing. The bonded chip carrier was then connected to a commercial DC source measuring unit (SM32P, FES Israel), which was controlled using an in-house data acquisition program. After setting the desirable source−drain voltage (V_{sd}) and the gate voltage (V_g), the source−drain (I_{sd}) was measured continuously while different solutions were introduced into the microfluidic channel. Figure 1a,b illustrates the design of the experimental setup.

RESULTS AND DISCUSSION

Aptamer-Modified SiNW-FET Surface Fabrication and Characterization. To facilitate the specific sensing of uranyl by the fabricated SiNW-FET devices, the SiNWs' surface was modified with a uranyl-specific aptamer. In order to confirm the successful immobilization of the aptamer, a 1 × 1 cm piece of the silicon wafer was modified in tandem with the actual device and characterized using X-ray photoelectron spectroscopy (XPS) following each modification step, Figure 1c (and Table S1). First, the surface was treated with oxygen plasma in order to clean and oxidize the silicon oxide surface in preparation for the silanization step. Then, the chip was covered with APDMES as a silanization agent, which introduced amine residues to the surface. Applying APDMES, under an argon atmosphere, is beneficial in creating a uniform silane monolayer,[51] which is essential for successful sensing in biological fluids. APDMES has shown enhanced stability to physiological conditions in comparison to other common silane modifiers.[52] XPS analysis confirmed the attachment of the amino-silane modifier, by presenting an increase in the percentage of nitrogen atoms. Following the activation of the carboxylic acid attached to the aptamer, with EDC and sulfo-NHS, the amine-modified surface was further reacted with the formed aptamer-NHS ester, in order to immobilize the aptamer by forming an amide bond. Finally, 3-hydroxypropionic acid was similarly activated and used to block any unreacted amine moieties on the surface of the SiNWs. The successful immobilization of the aptamer is clearly demonstrated by XPS analysis, with a corresponding increase in the atomic concentration of carbon and nitrogen, as well as the emergence of new nitrogen (N 1s) peaks, which can be attributed to the desired amide bond (NHC═O), and the C═N−C bond that is characteristic of adenine, guanine, and cytosine nitrogen bases (see Table S2 and Figure S2 for the N 1s XPS spectra, fitting, and bond population). Although phosphorous concentration might have been an excellent marker for DNA immobilization, the phosphorous peak is completely masked by silicon, and therefore cannot be quantified in the context of this analysis.

High Affinity toward Uranyl under Low Ionic Strength Conditions. After the successful immobilization of the uranyl-specific aptamer to the SiNW-FET, the fabricated chip was integrated into the electrical-measurement and sample-delivery systems. To evaluate the affinity of the bound aptamer to uranyl, the aptamer-modified SiNW-FET device was employed for measuring the electric response to increasing uranyl concentrations in low ionic strength SB. SiNW-FETs are sensitive to charged species adsorbed on their surface and experience a gating effect, causing an accumulation or depletion of charge-carriers within the SiNWs, thereby altering the conductivity through the SiNW. This results in an increase or decrease in the measured source−drain current

https://dx.doi.org/10.1021/acs.analchem.0c02387
Anal. Chem. 2020, 92, 12528−12537

(depending on the doping of the SiNW).[53] Upon dissociation of the adsorbed charged species from the SiNW's surface, the gating effect is removed, and the current is expected to return to its baseline level. Figure 2 depicts the device's response

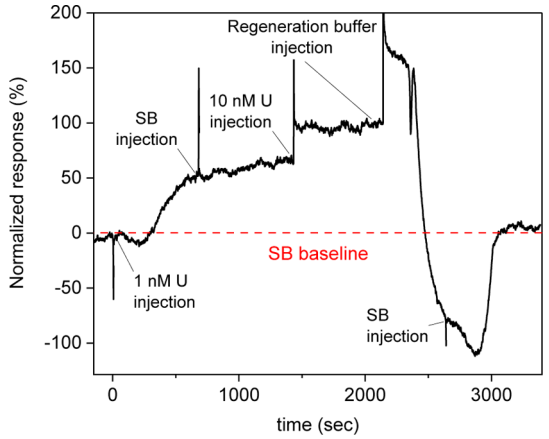

Figure 2. Real-time sensing of uranyl ions, using uranyl-binding aptamer-modified SiNW-FET, under low ionic strength conditions [sensing buffer (SB), 0.1 mM potassium phosphate buffer]. Indicated on the graph are points in time at which different solutions were introduced into the microfluidic channel.

during the course of the sensing experiment. First, low ionic strength SB was introduced into the microfluidic channel and a baseline current was established. A solution containing 1 nM of uranyl was then withdrawn into the microfluidic channel, leading to an increase in source−drain current, indicating uranyl binding by the immobilized aptamer. For p-type SiNWs, an increase in conduction is caused by a negative gating effect. Although uranyl is a positive ion, it is bound by a ssDNA aptamer, which has a negatively charged phosphate backbone and is much larger than the uranyl ion. It is, therefore, assumed that upon uranyl binding, the 3D structure of the aptamer changes, introducing more negatively charged DNA backbone moieties to the SiNW surface, thus changing the charge distribution on the surface and subsequently the conductivity of the SiNW. In FRET experiments performed on a derivative of the uranyl-binding aptamer,[54] it was found that for a high ionic strength (100 mM Na^+) the aptamer is folded to the most active configuration for uranyl binding, therefore, upon uranyl introduction, no further folding occurs and the uranyl binds by the "lock-and-key" mechanism. However, for a low ionic strength (30 mM Na^+), there are not enough positively charged species to resist the negative DNA backbone repulsion and stabilize this configuration, thus uranyl induces a local folding of the aptamer, leading to a more compact conformation. The starting point of all the experiments in our work is a low ionic strength environment, thus it is suggested that the aptamer undergoes a local fold, upon introduction of uranyl-containing samples into the microfluidic channel. It is possible that the induced folding brings the negatively charged DNA backbone close to the SiNW surface, thus inducing a negative gating effect—in coherence with the experimental results.

Alternating the solution back to SB, the current remained unchanged, not returning to its baseline level, suggesting a high affinity of the aptamer to uranyl. Further increasing the uranyl concentration to 10 nM uranyl did not yield a further increase in current, possibly because of saturation of binding sites. DNA aptamers are known for their high affinity and specificity toward their target and are, therefore, excellent candidates for various binding-based processes such as sensing, extraction, drug delivery, decontamination, and so forth. In the context of the uranyl-binding aptamer at hand,[18] its applicability as a uranyl-sequestering agent was demonstrated and strong binding to uranyl was observed. Such a high affinity required the use of 1 N HCl for the complete release of bound uranyl. Accordingly, in order to restore the uranyl-modified SiNW-FET baseline current, a regeneration buffer (HCl−glycine buffer, pH 3) was introduced into the microfluidic channel, causing a drastic current drop (because of the buffer's high ionic strength), and upon reintroduction of SB, the baseline current was regained.

Direct Sensing of Uranyl in Untreated Urine Samples.

Sensing the trace concentrations of ions and molecules in urine and other body fluids is hindered by the high ionic strength of these fluids, yielding a very short Debye length (~0.7 to 2.2 nm), which is readily exceeded by the mere length of the receptor and its linker. The short Debye-length restriction stems from the abundance of ions in biological samples, which surround the charged target molecule as it binds to the SiNWs. Through electrostatic interactions, the ions in the sample counteract the charge of the analyte, leading to a zero net charge. Thus, the gating effect induced by the charged target molecule is hampered, severely handicapping the sensitivity of the SiNW-FETs.

To overcome this limitation, a dissociation-regime sensing method was established,[24] in which the adsorption of the target analyte takes place upon the introduction of the sample to the receptor-modified SiNWs, while the measurement (i.e., sensing) is performed as the sample is being washed out by a low ionic strength buffer solution. During this stage, the nonspecifically bound matrix ions and other constituents readily dissociate from the SiNWs' surface, as opposed to the target molecule, which dissociates at a considerably slower rate, owing to its high affinity and specificity toward the immobilized receptor. This enables the temporal distinction between the measured electrical response toward the low-affinity matrix constituents and the high-affinity target molecule. The sensing scheme is depicted in Figure 3, demonstrating the low ionic strength SB baseline acquisition, followed by the adsorption stage in which the bio-sample is introduced to the SiNW-FET device and a change in response is observed (no analytical information can be obtained at this stage), and the final washing stage with low ionic strength SB results in the release of the bio-sample constituents while the uranyl ion remains bound by the specific uranyl-binding aptamer, leading to a different response from a nonspecific oligonucleotide-modified SiNW-FET in which both urine constituents and uranyl ions desorb without differentiation.

As previously shown,[24] in order to successfully achieve a temporal separation in the desorption of high- and low-affinity species, a strong-binding receptor is required. With the evidence of strong affinity toward uranyl displayed by the uranyl-binding aptamer, a dissociation regime sensing using the aptamer-modified SiNW-FET is expected to yield good results and overcome the screening effects from urine matrix constituents.

Aptamer-modified SiNW-FET was used for direct uranyl ion sensing in urine samples. Fresh undiluted urine was spiked with increasing uranyl acetate concentrations (final uranyl concentrations of 1 pM to 10 nM) and introduced into the

https://dx.doi.org/10.1021/acs.analchem.0c02387
Anal. Chem. 2020, 92, 12528−12537

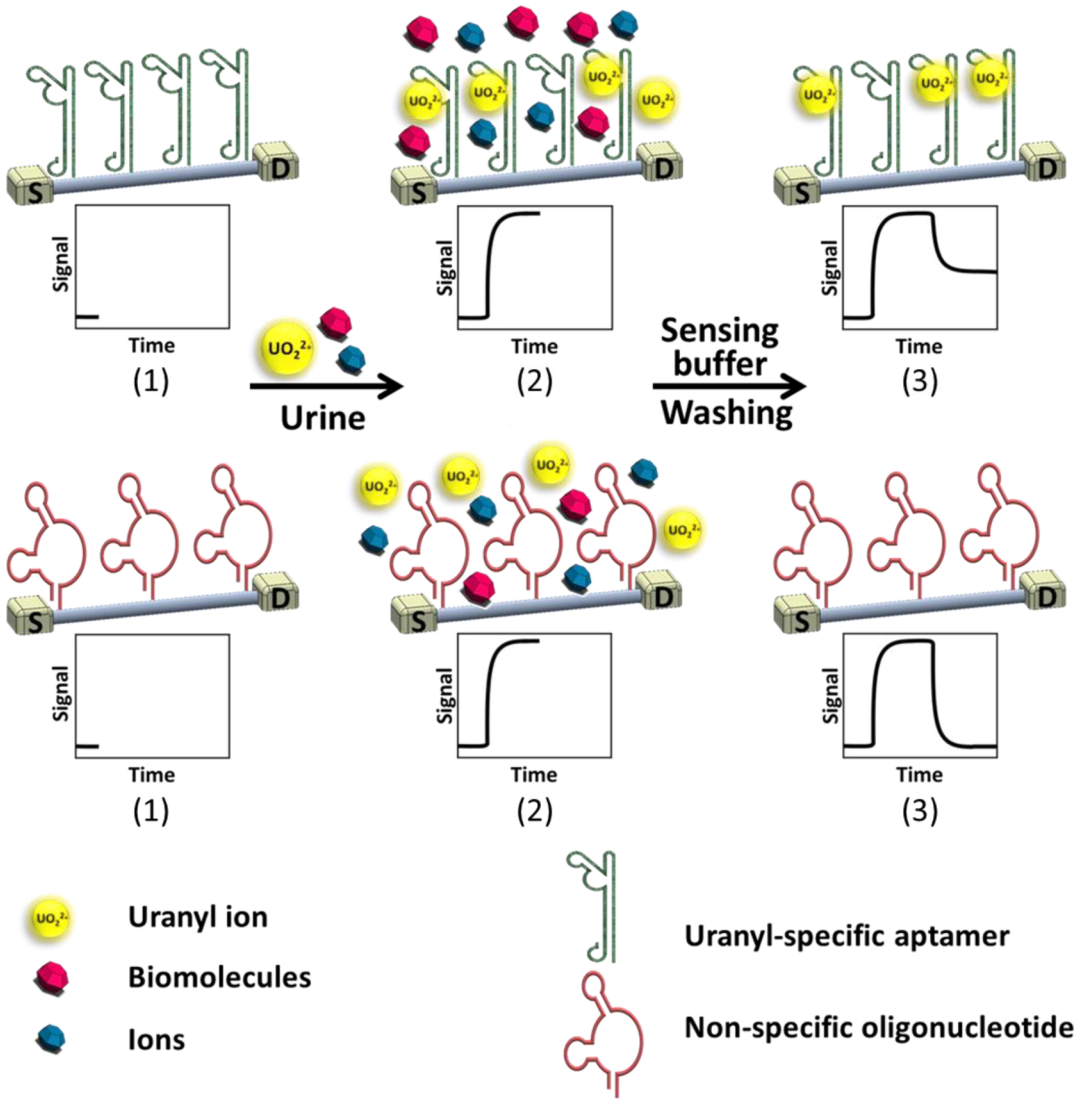

Figure 3. Schematic illustration of the operation of a uranyl-specific aptamer-modified SiNW-FET sensing device (upper scheme) vs a nonspecific oligonucleotide-modified SiNW-FET control device (lower scheme). (1) SiNW-FET devices are first exposed to low ionic strength SB, and a baseline electrical signal is acquired. (2) Introducing the uranyl-spiked urine sample to the devices causes a similar change in response, governed by the high ionic content of the sample, which screens the uranyl binding-related electrical signal. (3) Reintroducing low ionic strength SB easily washes out the nonspecifically bound urine constituents (lower scheme, part 3), while the specifically and strongly bound uranyl ion desorbs at a slower rate (upper scheme, part 3), yielding different dissociation kinetics, which enables the detection of uranyl in complex urine samples. The signal vs time plots are for illustration only.

microfluidic channel, alternating with low ionic strength SB, and the source−drain current was measured as a function of time, during both the binding and dissociation stages. Each urine sample was drawn through the microfluidic channel for 10 min, until achieving the association plateau, followed by a washing-out stage with low ionic strength SB. Figure 4a displays the concentration-dependent sensing of the uranyl ions in urine using the dissociation-regime mode approach at a flow rate of 15 μL/min, which was calculated according to the following formula[24]

$$\text{normalized response (\%)} = \frac{I_{SB} - I_t}{I_{SB}} \times 100\%$$

where I_t is the source−drain current at a given point in time during the measurement, and I_{SB} is the current measured in sensing buffer after full dissociation of an unspiked urine sample. It is noteworthy that urine samples are filtered using a plain 0.45 μm syringe filter with a cellulose acetate membrane, in order to remove debris that might precipitate on the SiNWs. Cellulose acetate is not inert to uranyl and may adsorb or complex the uranyl ion.[55,56] Preliminary measurements have shown that a single filter can retain at least 0.3 μmol of uranyl. Hence, urine samples, which normally contain tens of picomoles (per liter), are considered practically free of uranyl after filtration. Therefore, the added concentration of uranyl (spike) is referred to as the sample concentration. It is clear that for practical purposes, urine filtration will hamper uranyl detection in the real unspiked samples. Urine filtration is not mandatory for sensing by SiNW-FET devices, however, for this proof of concept, it was favorable because it prolonged the life of the devices, and enabled quantification of the devices' real detection limit.

Within the uranyl concentration range of 1 pM to 10 nM, the dissociation curves align from bottom to top with

https://dx.doi.org/10.1021/acs.analchem.0c02387
Anal. Chem. 2020, 92, 12528−12537

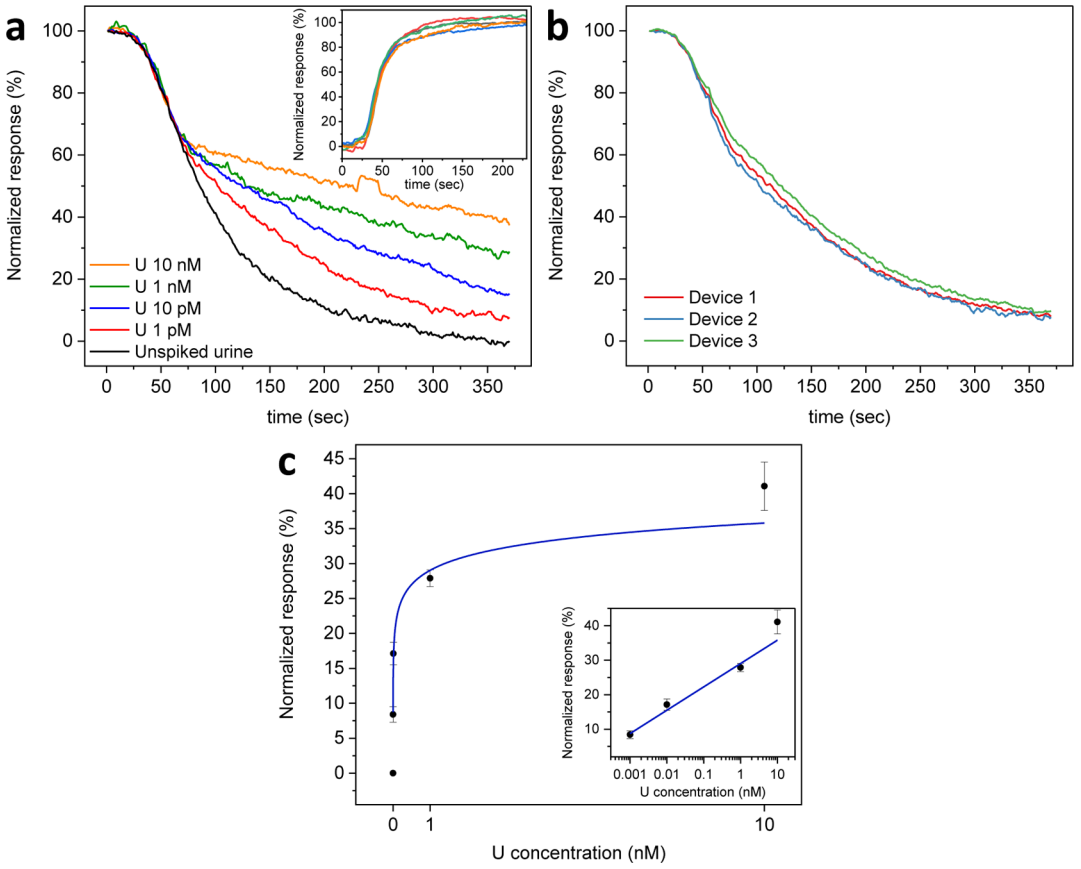

Figure 4. Uranyl ion sensing in urine samples. (a) Concentration-dependent sensing of uranyl ions in spiked urine samples, using the dissociation-regime mode approach at a flow rate of 15 μL/min. The black, red, blue, green, and orange curves show the normalized dissociation regime electrical response of the uranyl-binding aptamer-modified SiNW-FET sensing device for urine samples spiked with 0, 1 pM, 10 pM, 1 nM, and 10 nM uranyl, respectively. Each urine sample was drawn through the microfluidic channel for ∼10 min until achieving the association plateau. Inset: normalized response as a function of time, as measured during the binding period, for uranyl-spiked urine samples of matching concentrations. (b) Normalized dissociation-regime electrical response of three distinct uranyl-binding aptamer-modified SiNW-FET sensing devices for a urine sample spiked with 1 pM uranyl. The blue curve represents the same data as the red curve in (a). (c) Concentration-dependent calibration curve of the normalized response as a function of uranyl concentration in uranyl-spiked urine samples. The normalized response values after 370 s, as measured using three distinct devices, were extracted from the dissociation curves [(a) represents one of these devices], averaged, and plotted accompanied by the corresponding standard deviation. Inset: calibration data plotted against a logarithmic *X*-axis.

increasing concentrations, unlike the normalized electrical response measured during the binding stage (Figure 4a, inset), which exhibits no notable difference between solutions containing increasing uranyl concentrations. Using the calculated normalized responses, instead of absolute source–drain current values, reduces the device-to-device variation, which is a common drawback of SiNW-FETs. Thus, this normalization enhances the devices' reproducibility, as demonstrated by Figure 4b, which displays the dissociation curves of a 1 pM uranyl-spiked urine sample, as measured using three distinct devices. The blue curve is similar to the 1 pM curve from Figure 4a.

The normalized response measured after 370 s for each concentration was extracted from three distinct devices, averaged and plotted against the uranyl concentration. Figure 4c displays a clear correlation between the uranyl concentration and the device electrical response, thus demonstrating the aptamer-modified SiNW-FET capability to detect uranyl concentrations in a 4-orders of magnitude working range, with sensitivity as low as 1 pM (0.25 ng/L of U). The good reproducibility, especially among the lower concentrations, is further emphasized by the error bars, displaying the standard deviation of the calculated mean. Averaging the last 50 s of each dissociation curve (for uranyl-spiked samples) gives relative standard deviations in the range of 2−11% (see Figure S3), suggesting excellent device stability. The displayed sensitivity and stability are well suited for the determination of urinary uranyl levels in both unexposed and occupationally exposed populations.

In terms of specificity, the selection process of DNAzymes and aptamers, for example, systematic evolution of ligands by exponential enrichment (SELEX), usually addresses the issue of undesired affinity toward nontarget species by "counter SELEX" cycles,[57] which introduce nontarget molecules with a similar structure and discard oligonucleotides, which display affinity toward them, thereby increasing the specificity of the selected aptamer. The original uranyl-binding DNAzyme used in this work has shown high selectivity toward uranyl,[13] hence the derived aptamer is expected to follow the same trend. In the context of SiNW-FET devices, it is crucial to also eliminate nonspecific binding to the SiNWs, in order to prevent false-positive responses. Figure 5a depicts the dissociation curves of other heavy or toxic elements, as measured using an aptamer-modified SiNW device. The curves represent the normalized response of urine samples spiked with 10 nM of arsenic, cadmium, lead, zinc, and unspiked urine. It is clear that no

https://dx.doi.org/10.1021/acs.analchem.0c02387
Anal. Chem. 2020, 92, 12528−12537

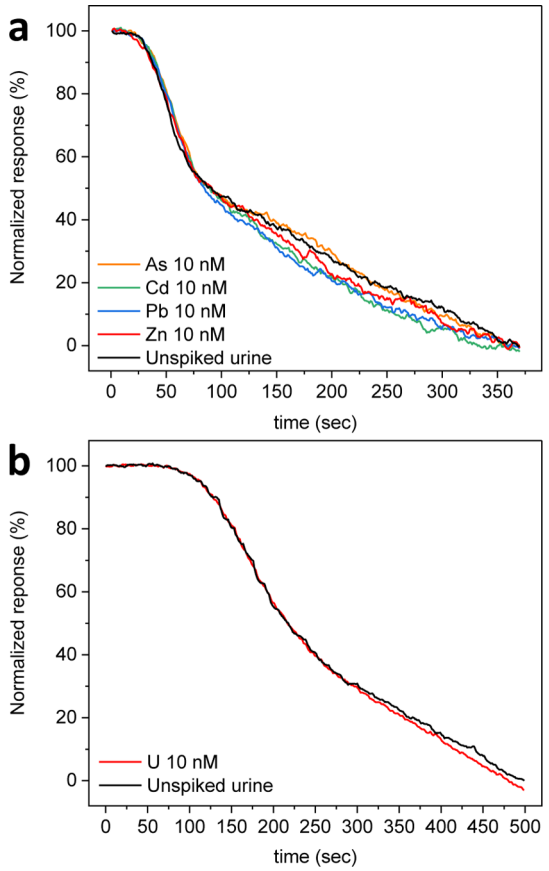

Figure 5. Control experiments for nonspecific binding. (a) Normalized response measured as a function of time during the dissociation period of urine samples spiked with toxic or heavy elements, using an aptamer-modified SiNW-FET device. The orange, green, blue, red, and black curves represent urine samples spiked with 10 nM of As, Cd, Pb, Zn, and unspiked urine, respectively. (b) Normalized response measured as a function of time during the dissociation period of urine samples using a nonspecific oligonucleotide-modified SiNW-FET device. The black curve represents an unspiked urine sample, whereas the red curve represents a urine sample spiked with 10 nM U.

notable binding has occurred, suggesting good specificity of the blocked SiNW surface itself. Given the lack of nonspecific binding displayed by the SiNWs, it is stressed that aptamer-modified SiNW-FET devices can serve as a universal, simple, real-time sensing method, limited only by the availability of high-affinity and selective aptamers toward a desired target metal ion. Until now, aptamers have been selected toward a broad range of targets, both chemical and biological,[58] and particularly against heavy metals and other toxic elements.[59−63] The availability of such a large pool of aptamers makes it possible to develop novel assay tools suitable for metal screening of either biological or environmental samples.

Finally, the response of a nonspecific oligonucleotide-modified SiNW-FET device to uranyl-spiked urine was examined. The oligonucleotide used was a single-strand DNA sequence of similar length to the uranyl-binding aptamer (117 bases), however, it contained only thymine bases. The experimental results are displayed in Figure 5b, which presents the dissociation curves for both unspiked (black curve) and spiked (10 nM U, red curve) urine samples. No notable response is observed suggesting a low affinity of uranyl toward a nonspecific oligonucleotide. This result highlights the importance of a target-specific receptor for the successful sensing of uranyl in the urine.

CONCLUSIONS

The aptamer-modified SiNW-FET presented in this work enables the simple and sensitive detection of uranyl in urine. The experimental approach employed in this work has a straight-forward implementation to other heavy and toxic metals, given the availability of target-specific aptamers. By shifting the analytical measurement to the dissociation stage, rather than the binding stage, the characteristic high ionic strength of urine samples becomes irrelevant, and sensitive detection with a picomolar concentration range is achieved. SiNW-FETs are known for notable device-to-device variations, which may hinder the reproducibility of the devices, and require the selection of quality devices prior to further modification. However, the normalization method employed in this work decreases this variation to an acceptable level. Nevertheless, contrary to the bottom-up fabrication method used herein, top-down processes may also be utilized to obtain higher intrinsic uniformity, thereby reducing the need for electrical characterization of each individual device, and allowing for only a small sample of each batch to be tested.

Owing to their reduced dimensions, SiNWs offer the ability to incorporate multiple sensors capable of detecting numerous chemical threats simultaneously on a single miniature array platform. Thus, SiNW-FETs have the potential to generate sensors with ultrahigh sensitivity, exceptional specificity toward a wide-range expandable "library" of detectable toxins, real-time detection, and portable easily operable devices. Combining the high surface-to-volume ratio of SiNWs, the high affinity and selectivity of the uranyl-binding aptamer, and the methodology of dissociation regime gives rise to a practical platform, offering simple and straightforward sensing of uranyl levels in urine, suitable for field deployment and point-of-care applications.

ASSOCIATED CONTENT

Supporting Information

The Supporting Information is available free of charge at https://pubs.acs.org/doi/10.1021/acs.analchem.0c02387.

Electrical characterization; XPS results including atomic concentrations, N 1s spectra with curve fitting, and bond population; device-to-device comparison for demonstrating stability and reproducibility (PDF)

AUTHOR INFORMATION

Corresponding Authors

Vadim Krivitsky − *School of Chemistry, the Raymond and Beverly Sackler Faculty of Exact Sciences, Tel Aviv University, Tel Aviv 69978, Israel*; Email: vadimkri@mail.tau.ac.il

Fernando Patolsky − *School of Chemistry, the Raymond and Beverly Sackler Faculty of Exact Sciences and Department of Materials Science and Engineering, the Iby and Aladar Fleischman Faculty of Engineering, Tel Aviv University, Tel Aviv 69978, Israel*; orcid.org/0000-0002-1382-5357; Email: fernando@post.tau.ac.il

Authors

Reut Meir − *School of Chemistry, the Raymond and Beverly Sackler Faculty of Exact Sciences, Tel Aviv University, Tel Aviv*

69978, Israel

Marina Zverzhinetsky − *School of Chemistry, the Raymond and Beverly Sackler Faculty of Exact Sciences, Tel Aviv University, Tel Aviv 69978, Israel*

Nimrod Harpak − *School of Chemistry, the Raymond and Beverly Sackler Faculty of Exact Sciences, Tel Aviv University, Tel Aviv 69978, Israel*

Ella Borberg − *School of Chemistry, the Raymond and Beverly Sackler Faculty of Exact Sciences, Tel Aviv University, Tel Aviv 69978, Israel*

Larisa Burstein − *Wolfson Applied Materials Research Center, Tel Aviv University, Tel Aviv 69978, Israel*

Offer Zeiri − *Department of Analytical Chemistry, Nuclear Research Center, Negev, Beer-Sheva 84190, Israel*

Complete contact information is available at: https://pubs.acs.org/10.1021/acs.analchem.0c02387

Notes

The authors declare no competing financial interest.

■ ACKNOWLEDGMENTS

This research was funded by the Pazy Foundation [joint foundation established by the Israeli University Planning and Budgeting Committee (UPBC) and the Israeli Atomic Energy Commission (IAEC)] Grants.

■ REFERENCES

(1) *Uranium 2018: Resources, Production and Demand; A Joint Report by the Nuclear Energy Agency and the International Atomic Energy Agency*; OECD Publications, 2019.

(2) Keith, S.; Faroon, O.; Roney, N.; Scinicariello, F.; Wilbur, S.; Ingerman, L.; Llados, F.; Plewak, D.; Wohlers, D.; Diamond, G. *Toxicological Profile for Uranium*; Agency for Toxic Substances and Disease Registry (US), 2013.

(3) Lestaevel, P.; Houpert, P.; Bussy, C.; Dhieux, B.; Gourmelon, P.; Paquet, F. *Toxicology* **2005**, *212*, 219−226.

(4) *Nuclear Forensics in Support of Investigation—Implementing Guide*; IAEA Nuclear Security Series; International Atomic Energy Agency (IAEA): Vienna, 2015; p 80.

(5) Okaneku, J.; Vearrier, D.; Mckeever, R.; Lasala, G.; Greenberg, M. I. *Clin. Toxicol.* **2015**, *53*, 931−934.

(6) Thakur, P.; Ward, A. L. *Health Phys.* **2019**, *116*, 694.

(7) Wu, X.; Huang, Q.; Mao, Y.; Wang, X.; Wang, Y.; Hu, Q.; Wang, H.; Wang, X. *TrAC, Trends Anal. Chem.* **2019**, *118*, 89−111.

(8) Shinkai, S.; Koreishi, H.; Ueda, K.; Arimura, T.; Manabe, O. *J. Am. Chem. Soc.* **1987**, *109*, 6371−6376.

(9) Boulet, B.; Bouvier-Capely, C.; Cossonnet, C.; Cote, G. *Solvent Extr. Ion Exch.* **2006**, *24*, 319−330.

(10) Sonoda, M.; Nishida, M.; Ishii, D.; Yoshida, I. *Anal. Sci.* **1999**, *15*, 1207−1213.

(11) Keener, M.; Hunt, C.; Carroll, T. G.; Kampel, V.; Dobrovetsky, R.; Hayton, T. W.; Ménard, G. *Nature* **2020**, *577*, 652−655.

(12) Wen, Y.; Yuan, Y.; Li, L.; Ma, D.; Liao, Q.; Hou, S. *Microchim. Acta* **2017**, *184*, 3909−3917.

(13) Liu, J.; Brown, A. K.; Meng, X.; Cropek, D. M.; Istok, J. D.; Watson, D. B.; Lu, Y. *Proc. Natl. Acad. Sci. U.S.A.* **2007**, *104*, 2056−2061.

(14) Brown, A. K.; Liu, J.; He, Y.; Lu, Y. *ChemBioChem* **2009**, *10*, 486−492.

(15) Lee, J. H.; Wang, Z.; Liu, J.; Lu, Y. *J. Am. Chem. Soc.* **2008**, *130*, 14217−14226.

(16) Zhang, H.; Cheng, X.; Chen, L.; Mo, F.; Xu, L.; Fu, F. *Anal. Chim. Acta* **2017**, *956*, 63−69.

(17) Zhou, B.; Shi, L.-F.; Wang, Y.-S.; Yang, H.-X.; Xue, J.-H.; Liu, L.; Wang, Y.-S.; Yin, J.-C.; Wang, J.-C. *Spectrochim. Acta, Part A* **2013**, *110*, 419−424.

(18) Kim, J.; Kim, M. Y.; Kim, H. S.; Hah, S. S. *Bioorg. Med. Chem. Lett.* **2011**, *21*, 4020−4022.

(19) Peretz-Soroka, H.; Pevzner, A.; Davidi, G.; Naddaka, V.; Tirosh, R.; Flaxer, E.; Patolsky, F. *Nano Lett.* **2013**, *13*, 3157−3168.

(20) Kwiat, M.; Elnathan, R.; Kwak, M.; de Vries, J. W.; Pevzner, A.; Engel, Y.; Burstein, L.; Khatchtourints, A.; Lichtenstein, A.; Flaxer, E.; Herrmann, A.; Patolsky, F. *J. Am. Chem. Soc.* **2012**, *134*, 280−292.

(21) Pevzner, A.; Engel, Y.; Elnathan, R.; Ducobni, T.; Ben-Ishai, M.; Reddy, K.; Shpaisman, N.; Tsukernik, A.; Oksman, M.; Patolsky, F. *Nano Lett.* **2010**, *10*, 1202−1208.

(22) Elnathan, R.; Kwiat, M.; Pevzner, A.; Engel, Y.; Burstein, L.; Khatchtourints, A.; Lichtenstein, A.; Kantaev, R.; Patolsky, F. *Nano Lett.* **2012**, *12*, 5245−5254.

(23) Krivitsky, V.; Hsiung, L.-C.; Lichtenstein, A.; Brudnik, B.; Kantaev, R.; Elnathan, R.; Pevzner, A.; Khatchtourints, A.; Patolsky, F. *Nano Lett.* **2012**, *12*, 4748−4756.

(24) Krivitsky, V.; Zverzhinetsky, M.; Patolsky, F. *Nano Lett.* **2016**, *16*, 6272−6281.

(25) Lefler, S.; Vizel, R.; Yeor, E.; Granot, E.; Heifler, O.; Kwiat, M.; Krivitsky, V.; Weil, M.; Yaish, Y. E.; Patolsky, F. *Nano Lett.* **2018**, *18*, 190−201.

(26) Patolsky, F.; Krivitsky, V.; Heifler, O.; Zverzhinetsky, M. Method and System for Subcutaneous Sensing. U.S. Patent 20,190,223,795 A1, July 25, 2019.

(27) Patolsky, F.; Krivitsky, V.; Zverzhinetsky, M. Method and System for Sensing by Modified Nanostructure. U.S. Patent 10,667,750 B2, June 2, 2020.

(28) Kwiat, M.; Cohen, S.; Pevzner, A.; Patolsky, F. *Nano Today* **2013**, *8*, 677−694.

(29) Krivitsky, V.; Zverzhinetsky, M.; Krivitsky, A.; Hsiung, L.-C.; Naddaka, V.; Gabriel, I.; Lefler, S.; Conroy, J.; Burstein, L.; Patolsky, F. *Nano Lett.* **2019**, *19*, 2478−2488.

(30) Borberg, E.; Zverzhinetsky, M.; Krivitsky, A.; Kosloff, A.; Heifler, O.; Degabli, G.; Soroka, H. P.; Fainaro, R. S.; Burstein, L.; Reuveni, S.; Diamant, H.; Krivitsky, V.; Patolsky, F. *Nano Lett.* **2019**, *19*, 5868−5878.

(31) Zheng, G.; Patolsky, F.; Cui, Y.; Wang, W. U.; Lieber, C. M. *Nat. Biotechnol.* **2005**, *23*, 1294−1301.

(32) Jain, K. K. *Clin. Chim. Acta* **2005**, *358*, 37−54.

(33) Burg, T. P.; Godin, M.; Knudsen, S. M.; Shen, W.; Carlson, G.; Foster, J. S.; Babcock, K.; Manalis, S. R. *Nature* **2007**, *446*, 1066−1069.

(34) Stern, E.; Wagner, R.; Sigworth, F. J.; Breaker, R.; Fahmy, T. M.; Reed, M. A. *Nano Lett.* **2007**, *7*, 3405−3409.

(35) Stern, E.; Vacic, A.; Reed, M. A. *IEEE Trans. Electron Devices* **2008**, *55*, 3119−3130.

(36) Patolsky, F.; Zheng, G.; Hayden, O.; Lakadamyali, M.; Zhuang, X.; Lieber, C. M. *Proc. Natl. Acad. Sci. U.S.A.* **2004**, *101*, 14017−14022.

(37) Patolsky, F.; Timko, B. P.; Yu, G.; Fang, Y.; Greytak, A. B.; Zheng, G.; Lieber, C. M. *Science* **2006**, *313*, 1100−1104.

(38) Engel, Y.; Elnathan, R.; Pevzner, A.; Davidi, G.; Flaxer, E.; Patolsky, F. *Angew. Chem., Int. Ed.* **2010**, *49*, 6830−6835.

(39) Lichtenstein, A.; Havivi, E.; Shacham, R.; Hahamy, E.; Leibovich, R.; Pevzner, A.; Krivitsky, V.; Davivi, G.; Presman, I.; Elnathan, R.; Engel, Y.; Flaxer, E.; Patolsky, F. *Nat. Commun.* **2014**, *5*, 4195.

(40) Livi, P.; Kwiat, M.; Shadmani, A.; Pevzner, A.; Navarra, G.; Rothe, J.; Stettler, A.; Chen, Y.; Patolsky, F.; Hierlemann, A. *Anal. Chem.* **2015**, *87*, 9982−9990.

(41) Cui, Y.; Wei, Q.; Park, H.; Lieber, C. M. *Science* **2001**, *293*, 1289−1292.

(42) Kim, J.; Rim, Y. S.; Chen, H.; Cao, H. H.; Nakatsuka, N.; Hinton, H. L.; Zhao, C.; Andrews, A. M.; Yang, Y.; Weiss, P. S. *ACS Nano* **2015**, *9*, 4572−4582.

(43) Krivitsky, V.; Zverzhinetsky, M.; Patolsky, F. *ACS Nano* **2020**, *14*, 3587.

(44) Banerjee, S.; Hsieh, Y.-J.; Liu, C.-R.; Yeh, N.-H.; Hung, H.-H.; Lai, Y.-S.; Chou, A.-C.; Chen, Y.-T.; Pan, C.-Y. *Small* **2016**, *12*, 5524−5529.
(45) Li, B.-R.; Hsieh, Y.-J.; Chen, Y.-X.; Chung, Y.-T.; Pan, C.-Y.; Chen, Y.-T. *J. Am. Chem. Soc.* **2013**, *135*, 16034−16037.
(46) Kim, K. S.; Lee, H.-S.; Yang, J.-A.; Jo, M.-H.; Hahn, S. K. *Nanotechnology* **2009**, *20*, 235501.
(47) Romhildt, L.; Zorgiebel, F.; Ibarlucea, B.; Vahdatzadeh, M.; Baraban, L.; Cuniberti, G.; Pregl, S.; Weber, W. M.; Mikolajick, T.; Opitz, J. Human α-Thrombin Detection Platform Using Aptamers on a Silicon Nanowire Field-Effect Transistor. *27th International Symposium on Power and Timing Modeling, Optimization and Simulation (PATMOS)*; IEEE: Thessaloniki, 2017; pp 1−4.
(48) Lee, H.-S.; Kim, K. S.; Kim, C.-J.; Hahn, S. K.; Jo, M.-H. *Biosens. Bioelectron.* **2009**, *24*, 1801−1805.
(49) Anand, A.; Liu, C.-R.; Chou, A.-C.; Hsu, W.-H.; Ulaganathan, R. K.; Lin, Y.-C.; Dai, C.-A.; Tseng, F.-G.; Pan, C.-Y.; Chen, Y.-T. *ACS Sens.* **2017**, *2*, 69−79.
(50) Patolsky, F.; Zheng, G.; Lieber, C. M. *Nat. Protoc.* **2006**, *1*, 1711−1724.
(51) Yadav, A. R.; Sriram, R.; Carter, J. A.; Miller, B. L. *Mater. Sci. Eng. C* **2014**, *35*, 283−290.
(52) Peled, A.; Pevzner, A.; Peretz Soroka, H.; Patolsky, F. *J. Nanobiotechnol.* **2014**, *12*, 7.
(53) Patolsky, F.; Lieber, C. M. *Mater. Today* **2005**, *8*, 20−28.
(54) He, Y.; Lu, Y. *Chem.—Eur. J.* **2011**, *17*, 13732−13742.
(55) Basta, A. H.; Hosny, W. M. *Polym. Degrad. Stab.* **1998**, *60*, 239−245.
(56) Singh, N.; Balasubramanian, K. *RSC Adv.* **2014**, *4*, 27691−27701.
(57) Zhuo, Z.; Yu, Y.; Wang, M.; Li, J.; Zhang, Z.; Liu, J.; Wu, X.; Lu, A.; Zhang, G.; Zhang, B. *Int. J. Mol. Sci.* **2017**, *18*, 2142.
(58) Bunka, D. H. J.; Stockley, P. G. *Nat. Rev. Microbiol.* **2006**, *4*, 588−596.
(59) Li, L.; Li, B.; Qi, Y.; Jin, Y. *Anal. Bioanal. Chem.* **2009**, *393*, 2051−2057.
(60) Gao, F.; Gao, C.; He, S.; Wang, Q.; Wu, A. *Biosens. Bioelectron.* **2016**, *81*, 15−22.
(61) Xu, W.; Zhou, X.; Gao, J.; Xue, S.; Zhao, J. *Electrochim. Acta* **2017**, *251*, 25−31.
(62) Wu, Y.; Zhan, S.; Wang, L.; Zhou, P. *Analyst* **2014**, *139*, 1550−1561.
(63) Kim, M.; Um, H.-J.; Bang, S.; Lee, S.-H.; Oh, S.-J.; Han, J.-H.; Kim, K.-W.; Min, J.; Kim, Y.-H. *Environ. Sci. Technol.* **2009**, *43*, 9335−9340.

https://dx.doi.org/10.1021/acs.analchem.0c02387
Anal. Chem. 2020, 92, 12528−12537